Chemistry–A European Journal
Research Article
doi.org/10.1002/chem.202301747
Chemistry Europe
European Chemical Societies Publishing
www.chemeurj.org

Hot Paper

Living Self-Assembly of Metastable and Stable Two-Dimensional Platelets from a Single Small Molecule

Chenglong Liao[+],[a, b] Yanjun Gong[+],[a, b] Yanxue Che[+],[c] Linfeng Cui,[d] Yangxin Liu,[a, b] Hongwei Ji,[a, b] Yifan Zhang,[a, b] Ling Zang,[e] Jincai Zhao,*[a, b] and Yanke Che*[a, b]

This study reports the design of a donor-acceptor (D-A) molecule with two fluorene units on each side of a benzothiadiazole moiety, which allows multiple intermolecular interactions to compete with one another so as to induce the evolution of the metastable 2D platelets to the stable 2D platelets during the self-assembly of the D-A molecule. Importantly, the living seeded self-assembly of metastable and stable 2D structures with precisely controlled sizes can be conveniently achieved using an appropriate supersaturated level of a solution of the D-A molecule as the seeded growth medium that can temporarily hold the almost-proceeding spontaneous nucleation from competing with the seeded growth. The stable 2D platelets with smaller area sizes exhibit higher sensitivity to gaseous dimethyl sulfide, illustrating that the novel living self-assembly method provides more available functional structures with controlled sizes for practical applications. The key finding of this study is that the new living methodology is separated into two independent processes: the elaborate molecular design for various crystalline structures as seeds and the application of a supersaturated solution with appropriate levels as the growth medium to grow the uniform structures with controlled sizes; this would make convenient and possible the living seeded self-assembly of rich 1D, 2D, and 3D architectures.

Introduction

As a powerful method for fabricating tunable one-dimensional (1D)[1] and two-dimensional (2D)[2] structures, living seeded self-assembly has attracted extensive attention. The most successful example of this method is the living crystallization-driven self-assembly of polymers pioneered by Manners and co-workers, using which many complex 1D[1e–f,3] and 2D[2d–g] structures with controlled sizes can be fabricated. By contrast, the living self-assembly of small molecules is merely limited to the fabrication of various 1D structures[1a–c,4] and has far less reach for the growth of uniform 2D structures.[2a] So far, retarding the spontaneous nucleation process to allow only seeded growth has been recognized to be the key to living self-assembly,[1d,4a,5] and certain effective methods, such as using kinetically metastable aggregates to decrease the monomer concentration in solutions,[1a–c,2a,4a–i] have been developed to slow down nucleation. Despite these accumulated understandings, small molecule systems still face a great challenge in growing uniform 2D structures,[2a] likely because of the difficulty in synchronously controlling the favorable growth in the first and second dimensions and unfavorable growth in the third dimension. Very recently, we reported the introduction of a coformer (n-alkyl alcohol) to connect a donor-acceptor (D-A) molecule in two dimensions via continuous hydrogen bonds, in which the nucleation kinetics were regulated using the solvent environments that further facilitated the living self-assembly of 2D platelets with controlled shapes and sizes.[2b–c] Although this coassembly approach represents a leap in constructing small molecule-based 2D structures via living self-assembly, the coformer (alcohols) incorporated is disadvantageous to certain optoelectronic properties such as photostability.[6] Therefore, developing new living self-assembly methodology to construct uniform and size-controlled 2D structures from single functional small molecules is highly desired but remains a great challenge.

Herein, a D-A molecule, **1** (Figure 1), bearing two fluorene units (the D group) on each side of a benzothiadiazole moiety (the A group) was designed; this D-A molecule was initially grown into metastable green-emissive 2D platelets and subsequently evolved into stable orange-emissive 2D platelets in

[a] C. Liao,[+] Y. Gong,[+] Y. Liu, Prof. Dr. H. Ji, Prof. Dr. Y. Zhang, Prof. Dr. J. Zhao, Prof. Dr. Y. Che
Key Laboratory of Photochemistry
CAS Research/Education Center for Excellence in Molecular Sciences
Institute of Chemistry
Chinese Academy of Sciences
Beijing 100190 (China)
E-mail: jczhao@iccas.ac.cn
ykche@iccas.ac.cn

[b] C. Liao,[+] Y. Gong,[+] Y. Liu, Prof. Dr. H. Ji, Prof. Dr. Y. Zhang, Prof. Dr. J. Zhao, Prof. Dr. Y. Che
University of Chinese Academy of Sciences
Beijing 100049 (China)

[c] Y. Che[+]
HT-NOVA Co., Ltd.
Zhuyuan Road, Shunyi District, Beijing 101312 (China)

[d] Prof. Dr. L. Cui
Hebei Key Laboratory of Organic Functional Molecules
College of Chemistry and Material Science
Hebei Normal University
Shijiazhuang 050023 (P. R. China)

[e] Prof. Dr. L. Zang
Nano Institute of Utah, and
Department of Materials Science and Engineering
University of Utah
Salt Lake City, Utah 84112 (United States)

[+] These authors contributed equally to this work.

Supporting information for this article is available on the WWW under https://doi.org/10.1002/chem.202301747

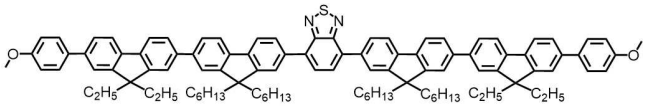

Figure 1. Molecular structure of **1**.

its spontaneous self-assembly. Crystallographic analyses show that the electrostatic attraction between **1** is the dominant force for the formation of metastable 2D platelets, whereas the combined π-interactions and electrostatic attraction between **1** drive the ultimate formation of the stable 2D platelets. Importantly, the living seeded self-assembly of metastable and stable 2D structures with uniform shapes and precise sizes can be achieved using an appropriate supersaturated level of a solution of **1** as the growth medium that can temporarily hold the almost-proceeding spontaneous nucleation of **1** to allow the only growth on the added seeds. This new methodology allows the living self-assembly of small molecules to proceed in two independent steps, thus being convenient to fabricate different 2D structures. To highlight the potential of the new living self-assembly method in optimizing the material properties, three batches of the metastable and stable 2D platelets with different area sizes were fabricated for the fluorescence detection of gaseous dimethyl sulfide (DMS), for which the stable 2D platelets with smaller area sizes exhibited the higher sensitivity to gaseous DMS. Because there is no requirement for the formation of metastable aggregates[1a–c,2a,4a–i] to restrict the fast nucleation as observed in the formation of 1D structures, this living self-assembly method, i.e., using an appropriate supersaturated solution to hold spontaneous nucleation, is convenient and adaptable to any crystallizable molecules toward different architectures.

Results and Discussion

Molecular Design

D-A molecule **1** with two fluorene units (donor) on each side of a benzothiadiazole moiety (acceptor) was designed as shown in Figure 1. The detailed synthesis procedures and characterizations of **1** are provided in the Supporting Information. Intermolecular interactions encoded in the molecular structure of **1** include electrostatic attraction and π-interactions that arise from the D-A backbone as well as dipole-dipole interactions between the polar methoxyphenyl groups at the molecular ends. Because the dipole-dipole interaction between polar methoxyphenyl groups and polar solvent[7] can compete with that of polar methoxyphenyl groups in between, applying a polar solvent (e.g., acetonitrile) in self-assembly of **1** would suppresses the epitaxial growth driven by the interactions between polar methoxyphenyl groups. This effect, together with relative strong electrostatic attraction and π-interactions in other directions, may lead to the formation of 2D structures.

Evolution of the Metastable 2D Platelets to the Stable 2D Platelets in the Self-Assembly of 1

Fluorescence microscopy was used to investigate the spontaneous self-assembly process of **1**, in which 5 mL of acetonitrile (poor solvent) was added into 1 mL of a chloroform solution of **1** (0.5 mg/mL) in a quartz cuvette to start the self-assembly at room temperature. Figure 2 shows the fluorescence-mode optical images of **1** in the resulting solvent mixture captured at an excitation wavelength of 330–390 nm (0.75 mW/mm^2), showing the time-dependent evolution of the assembly. At t = 0 min, i.e., immediately after adding acetonitrile into a chloroform solution of **1**, a homogeneous orange emission was observed in the entire solution (Figure 2a), assigned to the fluorescence of monomeric **1**. After about 60 min, the diamond-like 2D platelets began to appear in the solution (Figure 2b). The detailed process is clearly shown in Movie S1. Once formed, the diamond-like 2D platelets continued to grow and were accompanied by fading of the background emission (Figure 2c), indicative of the consumption of monomeric **1**. Notably, the resulting green-emissive 2D platelets exhibit a wide distribution in the area sizes ($A_w/A_n = 1.33$, where A_w is the weight-average area and A_n is the number-average area, see details in Figure S3), a typical phenomenon of spontaneous nucleation in self-assembly. At 600 min, the solution background became dark because of the consumption of free monomer **1**, while the diamond-like 2D platelets exhibited green emission without the disturbance of the background emission from monomers (Figure 2d). The change in absorption also shows the time-dependent evolution of the assembly (Figure 2e), i.e., the absorbance of **1** in a chloroform/acetonitrile mixture (v/v, 1/5; 0.083 mg/mL) remains unchanged for the first 40 min and then quickly decreases. The existence of a lag time, i.e., the first 40 min where the absorption of **1** remains unchanged, indicates the occurrence of a relatively slow nucleation process. After the lag time, the absorbance of **1** rapidly decreases (Figure 2e), indicating the autocatalytic growth of the diamond-like 2D platelets. The lag time of the self-assembly of **1** is dependent on the good/poor solvent ratio (Figures 2e and S4), i.e., decreasing with the increase of poor solvent component. For example, when **1** is self-assembled in a chloroform/acetonitrile (v/v, 1/3) mixture, the lag time is longer and when **1** is self-assembled in a chloroform/acetonitrile (v/v, 1/10) mixture, there is no lag time (Figure S4). These results show that the spontaneous nucleation rate of **1** can be tuned or temporarily suppressed using different solvent environments; this in turn suggests that it is feasible to create an appropriate supersaturation level (or regarded as a solution of almost-proceeding nucleation) to retard the nucleation process which may be used in living self-assembly.

Intriguingly, as time progressed, the green-emissive 2D platelets gradually disassembled and the orange-emissive hexagonal-like 2D platelets emerged and kept growing until the complete disappearance of the green-emissive 2D platelets after 3600 min (Figure 2f–i). Scanning electron microscopy (SEM) images revealed that the green-emissive 2D platelets first became rough at the edge (Figure 2l) and then broke into small

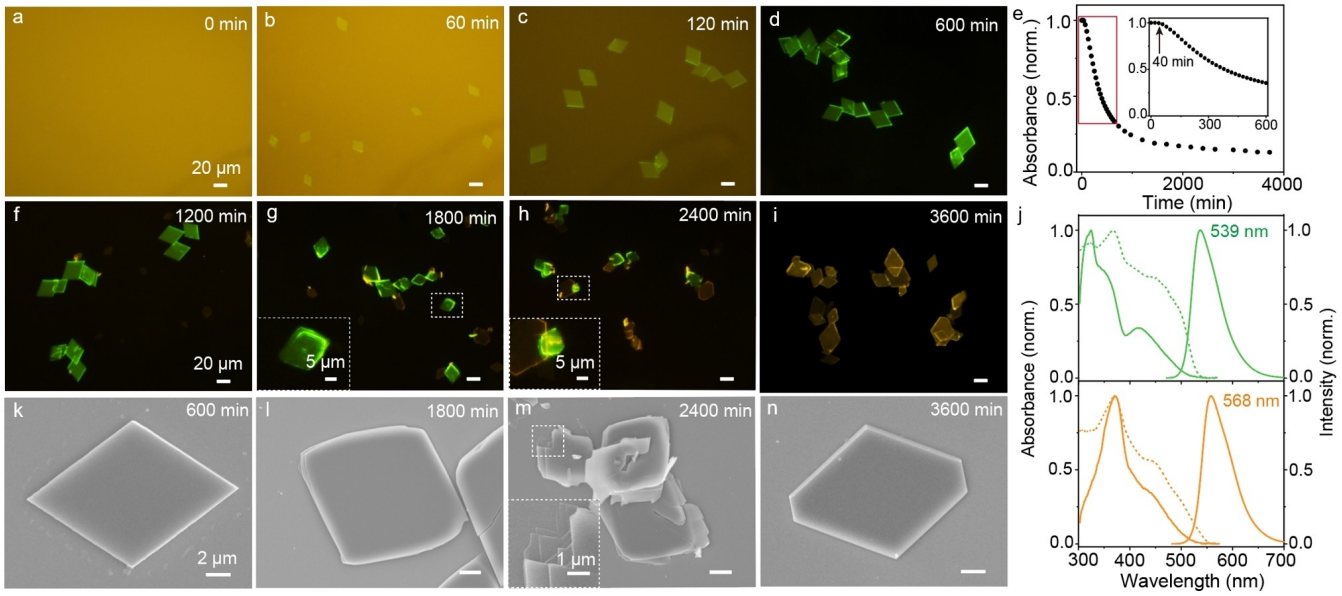

Figure 2. (a–d) Fluorescence-mode optical images of **1** in a chloroform/acetonitrile (v/v, 1/5) mixture showing the self-assembly of the metastable green-emissive 2D platelets. (e) Time-dependent absorbance of **1** at 350 nm in a chloroform/acetonitrile (v/v, 1/5) mixture. The inset is the absorbance of **1** within 600 min, showing a lag time of 40 min for the self-assembly. (f–i) Fluorescence-mode optical images showing the growth of the stable orange-emissive 2D platelets at the expense of the metastable green-emissive platelets in a chloroform/acetonitrile (v/v, 1/5) mixture. (j) UV-vis absorption (solid), excitation (dashed), and fluorescence spectra of the green-emissive and orange-emissive 2D platelets formed thereof. (k–m) SEM images of the green-emissive diamond-like 2D platelets formed at different self-assembly times. (n) SEM image of the final orange-emissive hexagonal-like 2D platelet. Of note, fluorescence images were recorded under UV excitation (330–390 nm, 0.75 mW/mm^2).

pieces (Figure 2m) during the growth of orange-emissive platelets. These observations indicate that the green-emissive 2D platelets are metastable aggregates that disassemble into monomers for the growth of the orange-emissive 2D platelets. Notably, the decomposition of the green-emissive 2D platelets and the growth of the orange-emissive 2D platelets were synchronically operating, as evidenced by the merely slightly decreased concentration of **1** during the shape transition (Figure 2e). The resulting orange-emissive platelets, which display a large area size dispersity, with an A_w/A_n value of 1.37 (Figure S3), underwent no further morphological change in weeks, indicative of their thermodynamically stable nature. Compared to the green-emissive 2D platelets, the orange-emissive 2D platelets exhibited slightly red-shifted absorption at long wavelengths (Figure 2j), indicating a larger degree of electron coupling of **1** in the orange-emissive 2D platelets than that in the green-emissive 2D platelets. In addition, analogous to the green-emissive 2D platelets, the excitation spectrum of the orange-emissive 2D platelets matches with the absorption spectra (Figure 2j), indicating that these 2D platelets undergo rapid relaxation to the lowest excited state to emit after excitation. SEM images revealed that both the metastable and stable 2D platelets had smooth and flat surfaces (Figures 2k and 2n). Their uniform thickness was further confirmed using atomic force microscopy (AFM) images (Figure S5).

Driving Forces behind the Evolution of the Self-Assembly of 1

The formation of the aforementioned distinct 2D structures correlates with different competitive interactions between **1**, which define the site depths in the energy landscape of self-assembly and thereby the self-assembly pathways.[8] To gain an insight into the intermolecular interactions in the two types of 2D platelets, single-crystal X-ray diffraction (SCXRD) analyses of the two types of 2D platelets were performed. Figures 3a and 3b show that molecule **1** in the metastable green-emissive 2D platelets undergoes different degrees of twisting between D and A units to afford four molecular conformations, which are contained in each crystal cell. The intermolecular distances of **1** along the a-axis and b-axis are 5.2 and 5.0 Å, respectively (Figure 3b), corresponding to electrostatic attraction between **1**. Without involving π-interactions in the green-emissive 2D platelets, electrostatic attraction is the dominant force that bring D-A molecules **1** together in two dimensions. However, electrostatic attraction between **1** has to compete with the relatively large steric hindrance between four twisting conformers of **1**; this consequently renders the green-emissive 2D platelets at a shallow position in the energy landscape, i.e., the formation of a metastable 2D state.[8] By contrast, molecule **1** in the stable orange-emissive 2D platelet had a single conformation with an almost rotational symmetric structure, in which the fluorene units at each side of the benzothiadiazole group adopt the same twisting angle relative to the benzothiadiazole group (Figures 3c and 3d). This conformation effectively reduced the steric hindrance of **1** once packed, and the intermolecular distances along the a-axis and b-axis were 4.0 and 5.0 Å,

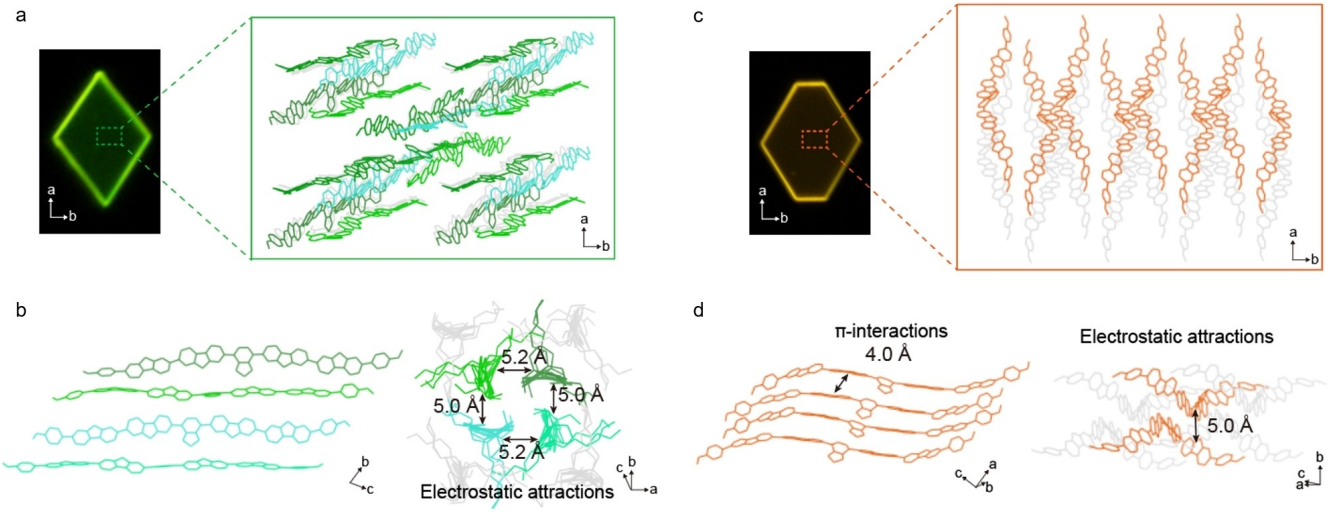

Figure 3. (a) Fluorescence-mode optical image and corresponding single-crystal structures of a green-emissive 2D platelet. Notably, the emerged bright edges of the 2D platelets arise from the optical waveguide effect. (b) 2D packing distances of molecule **1** with four different conformations in the green-emissive 2D platelet. (c) Fluorescence-mode optical image and corresponding single-crystal structures of an orange-emissive 2D platelet. (d) 2D packing distances of molecule **1** with a single conformation in the orange-emissive 2D platelet.

respectively (Figure 3d). The short intermolecular distance of 4.0 Å along the a-axis mirrors the weak π-interactions between **1**, whereas the longer molecular packing along the b-axis indicates the involvement of the electrostatic attractions. The weak π-interactions can enhance the electronic coupling between **1** and thereby contribute to slightly redshifted absorption and fluorescence spectra, as observed in Figure 2j. Furthermore, the emerging π-interactions can complement electrostatic attraction along the a-axis, rendering the orange-emissive 2D platelets at a deeper position in the energy landscape. This well explains the stable nature of the orange-emissive 2D platelets.

In addition, the crystalline structures of both metastable and stable 2D platelets reveal that the molecular packing of **1** along the thickness is driven by the interactions between the polar methoxyphenyl groups of **1** (Figure S6). This dipole-dipole interaction can be largely weakened by the competitive interaction of polar methoxyphenyl groups with acetonitrile, which thereby suppresses the epitaxial growth along the thickness. The weakened interaction along the thickness, together with strong electrostatic attraction in the other two dimensions, defines the formation of 2D structures above rather than 1D and 3D shapes.

Living Self-Assembly of Metastable and Stable 2D Platelets from 1

Having fabricated metastable and stable 2D platelets in which the formation is driven by different molecular interactions as described above, we next explored the possibility of living self-assembly of the two types of 2D platelets with controlled sizes. Inspired by the aforementioned observations that the spontaneous nucleation occurred slowly in certain solvent mixtures (Figures 2e and S4), we conjectured that the living seeded self-assembly of 2D platelets would be realized in a supersaturated solution of **1** with appropriate levels. The appropriate supersaturation solution can not only hold rapid spontaneous self-nucleation of **1** but also avoid its unnecessary solubility by excessive good solvent. To prove this hypothesis, the seeded self-assembly of **1** was studied in a supersaturated solution obtained by adding 5 mL of acetonitrile to 1 mL of a chloroform solution of **1** (0.1 mg/mL). Molecule **1** at this concentration (0.017 mg/mL) remained as individual monomers in this solvent mixture for 300 min and afterward began to quickly aggregate (Figure S7). Herein, the seed solution was added to the resulting supersaturated solution (Figure 4a) in the initial 180 min to ensure the virtual absence of spontaneous nucleation of **1**. Seeds as irregular fragments (Figure S8) were prepared by sonicating the prefabricated orange-emissive 2D platelets of **1** for 90 min at −35 °C (for details, see the Supporting Information). After the addition of a certain volume of seeds in acetonitrile (0.2 mg/mL) to the aforementioned supersaturated solution of **1** in a chloroform/acetonitrile (v/v, 1/5) mixture, the morphologies of the resulting 2D platelets were monitored and recorded by fluorescence microscopy. As shown in Figure 4b–e, very uniform orange-emissive 2D platelets are grown, for which the area dispersity was very low ($A_w/A_n = 1.01$, see details in Figure S9). Surprisingly, the growth process was very fast and finished in 15 min, which is in sharp contrast to the slow unseeded process as presented in Figure 2. The fast growth rules out the possible pathway via spontaneous nucleation, which otherwise would take as long as ~20 h (Figure 2). Quantitative analysis revealed that the areas of the resulting orange-emissive 2D platelets were proportional to the monomer-to-seed mass ratios (Figure 4f), characteristic of the living nature of the seeded self-assembly. Furthermore, the observed linear relationship suggests that the thickness of the orange-emissive 2D platelets with different area sizes remains almost constant during seeded growth. To confirm this, AFM imaging

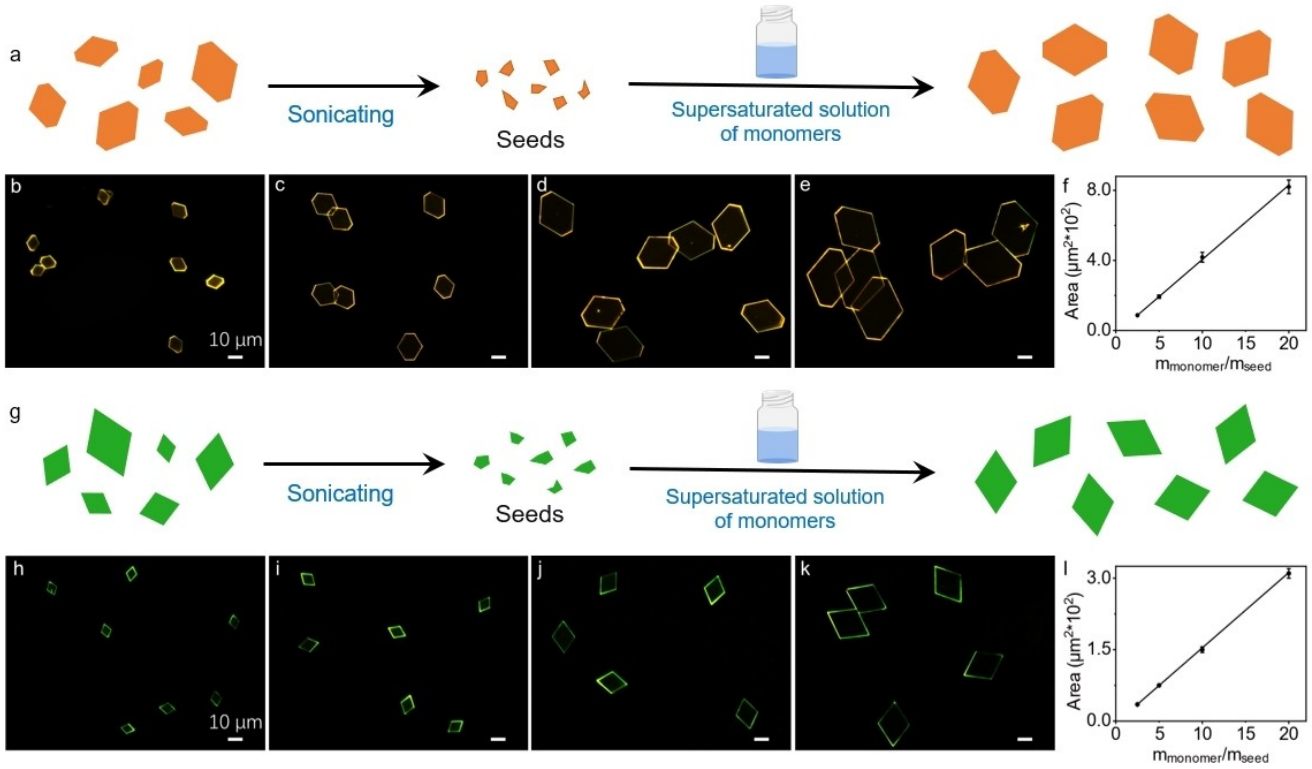

Figure 4. (a) Schematic representation of the living seeded self-assembly of the orange-emissive 2D platelets. (b–e) Fluorescence-mode optical images of the orange-emissive 2D platelets formed upon the addition of a certain volume of stable seeds (0.2 mg/mL) in acetonitrile to a supersaturated solution of **1** in a chloroform/acetonitrile (v/v, 1/5) mixture (6 mL, 0.017 mg/mL), at monomer-to-seed mass ratios ($m_{monomer}/m_{seed}$) of 2.5:1 (b), 5:1 (c), 10:1 (d), and 20:1 (e). (f) Area of the orange-emissive 2D platelets formed as a function of $m_{monomer}/m_{seed}$. (g) Schematic representation of the living seeded self-assembly of the green-emissive 2D platelets. (h-k) Fluorescence-mode optical images of the green-emissive 2D platelets formed upon the addition of a certain volume of metastable seeds (0.2 mg/mL) in acetonitrile to a supersaturated solution of **1** in a chloroform/acetonitrile (v/v, 1/5) mixture (1.2 mL, 0.083 mg/mL), at monomer-to-seed mass ratios of 2.5:1 (h), 5:1 (i), 10:1 (j), and 20:1 (k). (l) Area of the green-emissive 2D platelets formed as a function of $m_{monomer}/m_{seed}$. Of note, all 2D platelets were drop-cast on a glass substrate and excited by UV light (330–390 nm, 0.19 mW/mm^2).

was used to measure the thickness of the resulting orange-emissive 2D platelets. Figure S10 confirms that the thickness increases very slightly with the area size, falling within a narrow range of 200 to 230 nm. Further support for the living growth of 2D platelets came from the cyclic experiments (Figure S11) where sequential addition of 6 mL of **1** in the above supersaturated solution (0.017 mg/mL) to the seed solution (0.2 mL, 0.2 mg/mL) was conducted. Of note, 6 mL of the clean solution after each cycle of the living assembly was removed before the next addition. A linear relationship between the areas of the resulting orange-emissive 2D platelets and accumulated **1** in four cycles was observed (Figure S11), again consistent with the nature of living seeded growth. Intriguingly, the seeded self-assembly of 2D platelets took place at an accelerated rate with the subsequent cycles (Figure S12), which should result from the increased living sites with the enlarged circumference of 2D platelets. As expected, the very large orange-emissive 2D platelets (e.g., 119,855 μm^2) can be grown (Figure S13) by successively adding the supersaturated solution (0.017 mg/mL) of **1**. These results demonstrate that the living seeded self-assembly of 2D platelets from **1** is indeed realized using an appropriate supersaturated level of a solution as the growth medium that can effectively hold the spontaneous nucleation of **1**.

Given that metastable aggregates can restrict nucleation to create the conditions for living self-assembly as well,[2a] the metastable aggregate-mediated living self-assembly of the orange-emissive 2D platelets was carried out for comparison. Upon the addition of 0.2 mL of an acetonitrile solution of the orange-emissive seeds (0.2 mg/mL) to 1.2 mL of a chloroform/acetonitrile (v/v, 1/5) mixture containing the metastable green-emissive 2D platelets (0.083 mg/mL), the time-dependent morphological change was monitored and recorded by fluorescence microscopy. As shown in Figure S14, the orange-emissive 2D platelets gradually grew until the metastable green-emissive 2D platelets were completely disassembled and consumed within 25 h. The entire process resembles that shown in Figures 2g–i. The growth rate of the orange-emissive 2D platelets in this method is obviously much slower than that in the above supersaturated solution which was finished in 15 min. Furthermore, the 2D platelets formed by the metastable aggregate-mediated living self-assembly method have a wide area dispersity ($A_w/A_n > 1.31$, see details in Figure S15). This is likely because the disassembly rate of the metastable 2D platelets is too slow, thereby leading to uneven 2D growth of the seeds. The nonuniformity and slow growth unfolded in this method highlight the superiority of the living self-assembly

method using an appropriate supersaturated level of a solution as the seeded growth medium.

To explore the generality of the new approach, i.e., living self-assembly of different 2D structures in an appropriate supersaturated level of a solution, we applied it to the seeded growth of the metastable green-emissive 2D platelets with controlled sizes (Figure 4g). Notably, it remains less explored to fabricate metastable aggregates via living self-assembly. Analogous to the preparation of seeds for the orange-emissive 2D platelets, the seeds of the metastable 2D platelets (Figure S8) were prepared by sonicating the prefabricated green-emissive 2D platelets for 90 min at −35 °C. After adding a certain volume of seeds (0.2 mg/mL) in acetonitrile to the supersaturated solution of **1** (0.083 mg/mL) in a chloroform/acetonitrile (v/v, 1/5) mixture, the uniform green-emissive 2D platelets with a narrow area dispersity ($A_w/A_n = 1.01$) rapidly grew in 10 min (Figures 4h–k and S16), resembling the case of the orange-emissive 2D platelets (Figures 4b–e). Likewise, the areas of the resulting green-emissive 2D platelets are proportional to the monomer-to-seed mass ratios (Figure 4l), consistent with the only slightly increased thickness of the resulting green-emissive 2D platelets (within a range of 600 to 650 nm as shown in Figure S17). These results, together with a linear relationship between the areas of the green-emissive 2D platelets and accumulated **1** in four cycles (Figure S18 and S19), indicate the living seeded growth of the metastable green-emissive 2D platelets. Herein, the achievement of the living self-assembly of the metastable 2D platelets illustrates the versatility of this method, i.e., being not merely limited to growth of stable assemblies. Given the convenient and universal features, we anticipate that the independent two-step living methodology the living self-assembly reported herein would be extensible to other crystallizable molecules to construct shape-defined architectures beyond 2D.

Fluorescence Sensing of DMS Using Two Types of 2D Platelets

Given that the resulting two types of 2D platelets were highly emissive (Figure S20), we next applied them as fluorescence sensors for detecting chemicals of interest. Herein, DMS was chosen as the target analyte because it is a biomarker for diseases such as asthma and cystic fibrosis.[9] The two types of 2D platelets with three different area sizes (i.e., three batches) were grown using the aforementioned seeded self-assembly method and then applied to a previously reported detection device.[10] As shown in Figure 5a, the stable 2D platelets exhibited marked fluorescence-quenching responses when exposed to diluted gaseous DMS, such as 0.5 ppm DMS. The sulfur-π interactions[11] between **1** and DMS induce the quenching responses. As the area sizes of the stable 2D platelets increased, the extent of the fluorescence-quenching responses induced by DMS at the same concentrations significantly decreased, indicating a decrease in the sensitivity with area sizes of the stable 2D platelets. As expected, the smaller the sizes of the 2D platelets, the higher the sensitivity to DMS because of the increased surface area. The limit of detection (LOD) of these orange-emissive 2D platelets for DMS can be calculated using a previously applied method.[12] As shown in Figure 5b, the lowest LOD of 0.09 ppm was observed for the stable 2D platelets with the smallest area size (i.e., 20 μm^2). Importantly, the 2D platelets exhibited good selectivity to DMS against various common solvent interferents that caused no quenching responses under similar conditions (Figure S21).

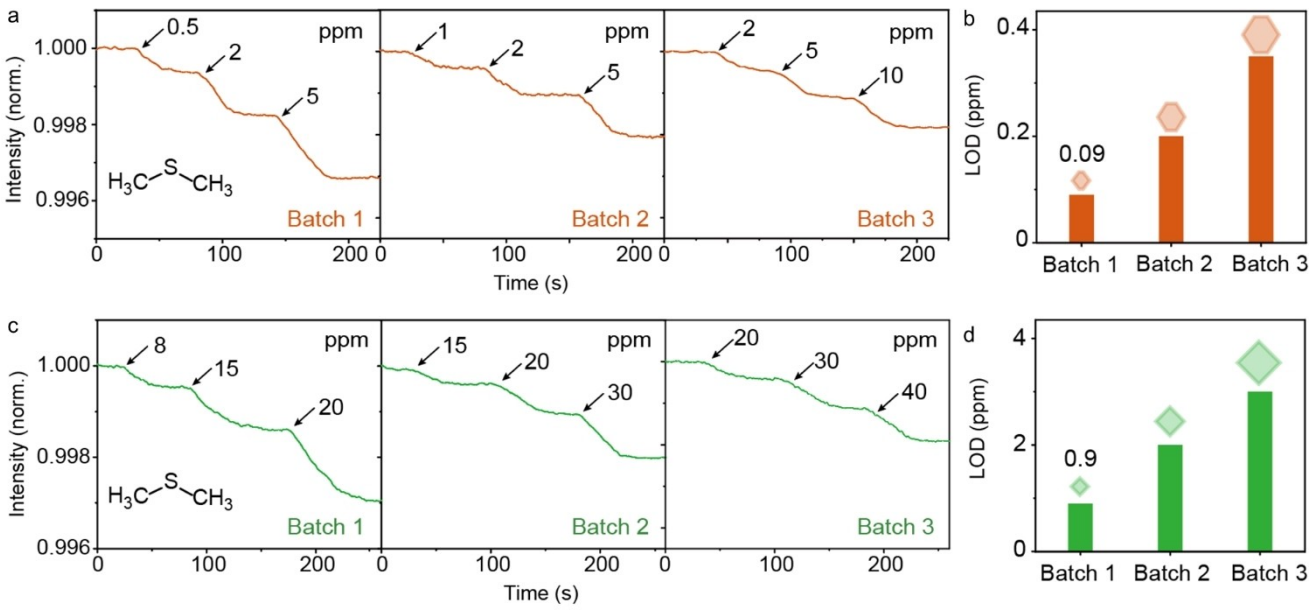

Figure 5. Fluorescence-quenching responses of three batches of the orange-emissive stable 2D platelets (a) and green-emissive metastable 2D platelets (c) to DMS at various concentrations (area size of the two types of 2D platelets: batch 1, 20 μm^2; batch 2, 200 μm^2; batch 3, 600 μm^2; area dispersity: $A_w/A_n < 1.02$). LOD values of the stable (b) and metastable (d) 2D platelets with different area sizes.

Analogous to the stable 2D platelets, the metastable 2D platelets exhibited area size-dependent sensitivity to gaseous DMS (Figure 5c). However, the LOD of the metastable 2D platelets was approximately 1 order of magnitude higher than that of the stable 2D platelets at the same area sizes (Figure 5b and 5d). For example, the lowest LOD of 0.9 ppm was observed on the metastable 2D platelets with the smallest area size (i.e., 20 μm^2) (Figure 5d). The decreasing sensitivity on the metastable 2D platelets is obviously related to the molecular packing, i.e., loose stacking is unfavorable for exciton diffusion within the platelet and in turn leads to smaller signal amplification. On the other hand, the π-interactions within the stable 2D platelets favor an overlap between the absorption and fluorescence spectra (Figure 2j), which facilitates exciton diffusion, resulting in higher signal amplification. Taken together, the above results point to the fact that the new living self-assembly method not only allows fabrication of more tunable functional structures for potential applications, but also enables secondary optimization of the properties of the resulting structures by precisely controlling their sizes.

Conclusions

In conclusion, we report the fabrication of two types of 2D platelets via the self-assembly of a rationally designed D-A molecule, in which the metastable green-emissive 2D platelets gradually convert into the stable orange-emissive 2D platelets. On the basis of single-crystal analyses, different competitive interactions are recognized to determine the formation of the two types of 2D platelets. Importantly, living seeded self-assembly of the two types of uniform 2D platelets with precisely controlled sizes can be achieved by applying an appropriate supersaturated level of a solution as the growth medium. As well illustrated in the fluorescence of trace DMS, the new living self-assembly method not only creates more tunable functional structures for applications, but also secondarily optimizes the properties of the grown materials by precisely controlling their sizes. Finally, we anticipate that the finding, i.e., separating the living methodology into two independent processes, would be a convenient and adaptable methodology for the living seeded self-assembly of novel architectures with controlled shapes and sizes.

Experimental Section

Synthesis details of molecule **1**, preparation of 2D platelets, optical and structural characterizations, and experimental details of fluorescence sensing can be found in the Supporting Information. Deposition Numbers 2261025 (for green-emissive 2D platelet), 2261026 (for orange-emissive 2D platelet) contain the supplementary crystallographic data for this paper. These data are provided free of charge by the joint Cambridge Crystallographic Data Centre and Fachinformationszentrum Karlsruhe Access Structures service.

Supporting Information

The authors have cited additional references within the Supporting Information.[2b,e,10,11]

Acknowledgements

This work was funded by National Key Research and Development Program of China (No. 2019YFA0210401, 2022YFA1205501, and 2022YFA1206200), NSFC (Nos. 21925604, 22275196), and the Strategic Priority Research Program of Chinese Academy of Sciences (Grant No. XDB36000000).

Conflict of Interests

The authors declare no conflict of interest.

Data Availability Statement

The data that support the findings of this study are available in the Supporting Information of this article.

Keywords: fluorescence sensor · living self-assembly · supersaturated solution · two-dimensional platelet

[1] a) N. Fukaya, S. Ogi, H. Sotome, K. J. Fujimoto, T. Yanai, N. Bäumer, G. Fernández, H. Miyasaka, S. Yamaguchi, *J. Am. Chem. Soc.* **2022**, *144*, 22479–22492; b) S. Ogi, K. Sugiyasu, S. Manna, S. Samitsu, M. Takeuchi, *Nat. Chem.* **2014**, *6*, 188–195; c) X. Ma, Y. Zhang, Y. Zhang, Y. Liu, Y. Che, J. Zhao, *Angew. Chem. Int. Ed.* **2016**, *55*, 9539–9543; d) J. Kang, D. Miyajima, T. Mori, Y. Inoue, Y. Itoh, T. Aida, *Science* **2015**, *347*, 646–651; e) X.-H. Jin, M. B. Price, J. R. Finnegan, C. E. Boott, J. M. Richter, A. Rao, S. M. Menke, R. H. Friend, G. R. Whittell, I. Manners, *Science* **2018**, *360*, 897–900; f) S. Shin, F. Menk, Y. Kim, J. Lim, K. Char, R. Zentel, T.-L. Choi, *J. Am. Chem. Soc.* **2018**, *140*, 6088–6094.

[2] a) T. Fukui, S. Kawai, S. Fujinuma, Y. Matsushita, T. Yasuda, T. Sakurai, S. Seki, M. Takeuchi, K. Sugiyasu, *Nat. Chem.* **2017**, *9*, 493–499; b) Y. Gong, C. Cheng, H. Ji, Y. Che, L. Zang, J. Zhao, Y. Zhang, *J. Am. Chem. Soc.* **2022**, *144*, 15403–15410; c) L. Fu, Y. Che, Y. Gong, H. Ji, Y. Zhang, L. Zang, J. Zhao, Y. Che, *Chem. Mater.* **2023**, *35*, 1310–1317; d) N. Yun, C. Kang, S. Yang, S.-H. Hwang, J.-M. Park, T.-L. Choi, *J. Am. Chem. Soc.* **2023**, *145*, 9029-9038; e) X. He, M.-S. Hsiao, C. E. Boott, R. L. Harniman, A. Nazemi, X. Li, M. A. Winnik, I. Manners, *Nat. Mater.* **2017**, *16*, 481–488; f) H. Qiu, Y. Gao, C. E. Boott, O. E. C. Gould, R. L. Harniman, M. J. Miles, S. E. D. Webb, M. A. Winnik, I. Manners, *Science* **2016**, *352*, 697–701; g) G. Chen, G. Zhang, B. Jin, M. Luo, Y. Luo, S. Aya, X. Li, *J. Am. Chem. Soc.* **2019**, *141*, 15498–15503.

[3] a) J. R. Finnegan, X. He, S. T. G. Street, J. D. Garcia-Hernandez, D. W. Hayward, R. L. Harniman, R. M. Richardson, G. R. Whittell, I. Manners, *J. Am. Chem. Soc.* **2018**, *140*, 17127–17140; b) M. C. Arno, M. Inam, Z. Coe, G. Cambridge, L. J. Macdougall, R. Keogh, A. P. Dove, R. K. O'Reilly, *J. Am. Chem. Soc.* **2017**, *139*, 16980–16985; c) B. Adelizzi, N. J. Van Zee, L. N. J. De Windt, A. R. A. Palmans, E. W. Meijer, *J. Am. Chem. Soc.* **2019**, *141*, 6110–6121; d) B. Jin, Q. Li, L. Hu, Q. Liu, Y. Chen, Y. Luo, S. Chi, X. Li, *Angew. Chem. Int. Ed.* **2023**, *135*, e202219067; e) J. Nie, X. Huang, G. Lu, M. A. Winnik, C. Feng, *Macromolecules* **2022**, *55*, 7856–7868; f) D. Bousmail, P. Chidchob, H. F. Sleiman, *J. Am. Chem. Soc.* **2018**, *140*, 9518–9530.

[4] a) H. Choi, S. Ogi, N. Ando, S. Yamaguchi, *J. Am. Chem. Soc.* **2021**, *143*, 2953–2961; b) S. Ogi, V. Stepanenko, J. Thein, F. Würthner, *J. Am. Chem. Soc.* **2016**, *138*, 670–678; c) P. Khanra, A. K. Singh, L. Roy, A. Das, *J. Am. Chem. Soc.* **2023**, *145*, 5270–5284; d) R. Laishram, S. Sarkar, I. Seth, N.

Khatun, V. K. Aswal, U. Maitra, S. J. George, *J. Am. Chem. Soc.* **2022**, *144*, 11306–11315; e) A. Aliprandi, M. Mauro, L. De Cola, *Nat. Chem.* **2016**, *8*, 10–15; f) Y. Liu, C. Peng, W. Xiong, Y. Zhang, Y. Gong, Y. Che, J. Zhao, *Angew. Chem. Int. Ed.* **2017**, *56*, 11380–11384; g) I. Helmers, G. Ghosh, R. Q. Albuquerque, G. Fernández, *Angew. Chem. Int. Ed.* **2021**, *60*, 4368–4376; h) Q. Wan, W.-P. To, X. Chang, C.-M. Che, *Chem* **2020**, *6*, 945–967; i) S. Sarkar, A. Sarkar, A. Som, S. S. Agasti, S. J. George, *J. Am. Chem. Soc.* **2021**, *143*, 11777–11787; j) E. E. Greciano, B. Matarranz, L. Sánchez, *Angew. Chem. Int. Ed.* **2018**, *57*, 4697–4701; k) D. Zhang, J. De, Y. Lei, H. Fu, *Nat. Commun.* **2021**, *12*, 1838.

[5] A. T. Haedler, S. C. J. Meskers, R. H. Zha, M. Kivala, H.-W. Schmidt, E. W. Meijer, *J. Am. Chem. Soc.* **2016**, *138*, 10539–10545.

[6] Y. Gong, L. Fu, Y. Che, H. Ji, Y. Zhang, L. Zang, J. Zhao, Y. Che, *J. Am. Chem. Soc.* **2023**, *145*, 9771–9776.

[7] W. Jin, Y. Yamamoto, T. Fukushima, N. Ishii, J. Kim, K. Kato, M. Takata, T. Aida, *J. Am. Chem. Soc.* **2008**, *130*, 9434–9440.

[8] F. Tantakitti, J. Boekhoven, X. Wang, R. V. Kazantsev, T. Yu, J. Li, E. Zhuang, R. Zandi, J. H. Ortony, C. J. Newcomb, L. C. Palmer, G. S. Shekhawat, M. O. de la Cruz, G. C. Schatz, S. I. Stupp, *Nat. Mater.* **2016**, *15*, 469–476.

[9] a) S. Awano, Y. Takata, I. Soh, A. Yoshida, T. Hamasaki, K. Sonoki, T. Ohsumi, T. Nishihara, T. Ansai, *J. Breath Res.* **2011**, *5*, 046007; b) M. Barker, M. Hengst, J. Schmid, H.-J. Buers, B. Mittermaier, D. Klemp, R. Koppmann, *Eur. Respir. J.* **2006**, *27*, 929–936.

[10] X. Du, Y. Gong, Y. Ren, L. Fu, R. Duan, Y. Zhang, Y. Zhang, J. Zhao, Y. Che, *Anal. Chem.* **2022**, *94*, 16418–16426.

[11] X. Yu, Y. Gong, H. Ji, C. Cheng, C. Lv, Y. Zhang, L. Zang, J. Zhao, Y. Che, *ACS Sens.* **2022**, *7*, 1395–1402.

[12] L. Cui, Y. Gong, X. Yu, C. Lv, X. Du, J. Zhao, Y. Che, *ACS Sens.* **2021**, *6*, 2851–2857.

Manuscript received: June 1, 2023
Accepted manuscript online: October 10, 2023
Version of record online: November 7, 2023